Regular Article

PHYSICAL CHEMISTRY RESEARCH
Published by the
Iranian Chemical Society
www.physchemres.org
info@physchemres.org

***Phys. Chem. Res.**, Vol. 5, No. 1, 81-98, March 2017*
DOI: 10.22036/pcr.2017.38495

New Activated Carbon from Persian Mesquite Grain as an Excellent Adsorbent

E. Ghasemian Lemraski*, S. Sharafinia and M. Alimohammadi
Faculty of Science, Ilam University, P.O. Box: 69315516, Ilam, Iran
(Received 8 July 2016, Accepted 2 October 2016)

This paper presents a systematic study of the surface chemistry, porous texture and adsorptive characteristics of a newly prepared activated carbon using Persian mesquite grain. Several techniques and methodologies such as, proximate analysis, N_2 adsorption-desorption isotherms, scanning electron microscope (SEM), Fourier transform infrared spectroscopy (FT-IR), X-ray Diffraction (XRD), X-ray photoelectron spectroscopy (XPS), temperature programmed desorption (TPD), Thermo gravimetric analysis TGA/DTA, elemental analysis (CHNS), Boehm titration, and point of zero charge (pH_{pzc}) have been used to determine the physicochemical properties of raw material and activated carbon, respectively. The prepared activated carbon has been also used to remove methyl orange (MO) and methylene blue (MB) as anionic and cationic azo dyes.

Keywords: Activation, X-ray photoelectron spectroscopy, Micro pore, Point of zero charge, Surface functional group

INTRODUCTION

The activated carbons (or ACs) are porous materials containing a high surface area and an appreciable amount of active sites available for adsorption of certain pollutants. Commercial production of activated carbon in recent times has been performed by the physical or chemical activation of a wide variety of materials [1-5].

In this work, preparation of the activated carbon from Persian prosopis farcta by chemical activation is presented. Proximate analysis, elemental analysis, FT-IR, XRD, Scanning electron microscopy (SEM) and TG/DTA have been performed to understand the structural changes during the process. Textural parameters were evaluated by N_2 adsorption. In our country traditionally raw materials such as shell walnuts, pistachios, baste joy, acorn caps, core fruit, and cereal waste have been used to produce activated carbon. However, Cork structure of Persian Mesquite Grain could be a new natural source to prepare activated carbon. Persian Mesquite Grain or Persian Prosopis Farcta is a short perennial foliage bush whose length often reaches 40-100 cm.

This work also focuses on the study of methyl orange (MO) and methylene blue (MB) removal from aqueous solution using activated carbon. In developing countries such as Iran water pollution is caused by industrial and municipal wastewater, as well as by agriculture. Except a few cases, there are no factory, industry and sewage disposal system in the country, especially in metropolitan areas.

Azo dyes, a type of textile colorants, are integral to the textile industry and make up 70% of commercial dyes. Research has shown that some Azo dyes pose very serious health risks to humans if they are used in particular textiles and if they get into retains water supplies. Azo dyes have been shown to damage ecosystems when are charged into water systems by dyeing factories, predominantly in developing countries. In 2002, the EU responded by banning Azo dyes that could break down to one of any of 24 possible carcinogenic products. There is a little equivalent regulation for potentially more serious wastewater contamination [6].

AC in the present work showed good monolayer adsorption capacity for MO and for MB, acceptable value to

*Corresponding author. E-mail: e.ghasemian@Ilam.ac.ir

the other granular and powdered activated carbons reported in the literatures. Various operational parameters like initial concentration, pH, time and temperature was optimized and reported.

EXPERIMENTAL

Materials

All used chemicals in this study, such as H_3PO_4 (99%), HCl (99%), methyl orange (MO), and methylene blue (MB), with high purity purchased from Merck (Darmstadt, Germany).

Preparation of Activated Carbon

Dried raw materials were mixed with H_3PO_4 solution at the H_3PO_4/C mass ratios of 1-1, and the mixture was dried at 105 °C for 12 h. The obtained material was pyrolyzed in a stainless steel reactor at a rate of 7 (°C min^{-1}) to 600 °C for 2 h and maintained for 100 min under N_2 flow protection. After cooling, the activated carbon was boiled with 200 ml of 10% HCl solution for 60 min, separated by filtration, and washed with water to eliminate the inorganic species. For the last step, the activated carbon was dried in an oven at 110 °C for 24 h.

INSTRUMENTS

The absorption studies were carried out using Jusco (Japan) UV-Vis spectrophotometer model V-570. The surface morphology of samples was investigated by scanning electron microscope (SEM, VEGA model, TESCAN Company, Czech). Fourier transform infrared (FTIR) spectra of samples were obtained using a spectrophotometer (Bruker-Germany VBRTEX70).

The composition of C, H and N in the activated carbon was determined using an elemental analyzer (PE-2400 II, Perkin-Elmer Corp., USA). The BET surface area measurements were obtained from nitrogen adsorption isotherms using a Micrometrics Surface Area Analyzer (Chem BET-3000, Quantachrom C., USA). X-ray diffraction analysis was performed by Philips PW1800 X-pert. Experiments were performed on a Perkin Elmer TGA Piers' 1 analyzer. XPS analysis was performed at CEMUP (Centro de Materiais da Universidade do Porto) with a VG Scientific ESCALAB 200A spectrometer. A Boehm method was used for the calculation of the number of acidic and basic groups on the particles' surfaces [6].

Batch Adsorption Experiments

The stock solution of dye was prepared in a flask with an adsorbent concentration of 0.05 g/25 ml; all of the adsorption experiments were carried out at 175 rpm in an orbital shaker. The dye concentration was measured within a time range of 5-80 min until equilibrium was reached. Effect of pH has been performed between pH 2-10. The experiments with the adsorption isotherms were conducted in a solution at pH 2.0, initial dye concentrations ranging from 150-300 (mg l^{-1}), t = 20 min, T = 303 K, and 175 rpm for MO and pH 6.0, initial dye concentrations ranging from 50-200 (mg l^{-1}), t = 20 min, T = 303 K, and 175 rpm for MB.

The following equation was used to calculate the removal percentage:

$$\%dye\ removal = \frac{C_0 - C_t}{C_0} \times 100 \quad (1)$$

where C_0 (mg l^{-1}) and C_t (mg l^{-1}) are the initial and final concentrations of dye, respectively. The maximum adsorbed amount at equilibrium, (q_e (mg g^{-1})), was calculated according to Eq. (2):

$$q_e = \frac{(C_0 - C_e)V}{W} \quad (2)$$

where C_e (mg l^{-1}) represents the equilibrium liquid-phase concentrations of dye, V (l) is the volume of the solution, and W (g) is the adsorbent mass.

RESULTS AND DISCUSSION

Characterization of Activated Carbon

Results of proximate and elemental analyses of the raw material are given in Table 1. The high fixed carbon and low ash content of the raw material is suitable for activation. Generally ash content of good activated carbon is in the range of 2-10% [7-9]. Also CHNS results show the carbon content of raw material is lower than that of the activated carbon. Results obtained in this study are close to the earlier

Table 1. Physicochemical Analysis of Prepared Activated Carbon

Elemental analysis	
C	37.65
N	0.570
H	4.360
O	57.42
Proximate analysis	
Moisture	2.601
Volatile matter	36.27
Fixed carbon	56.33
Ash	4.801

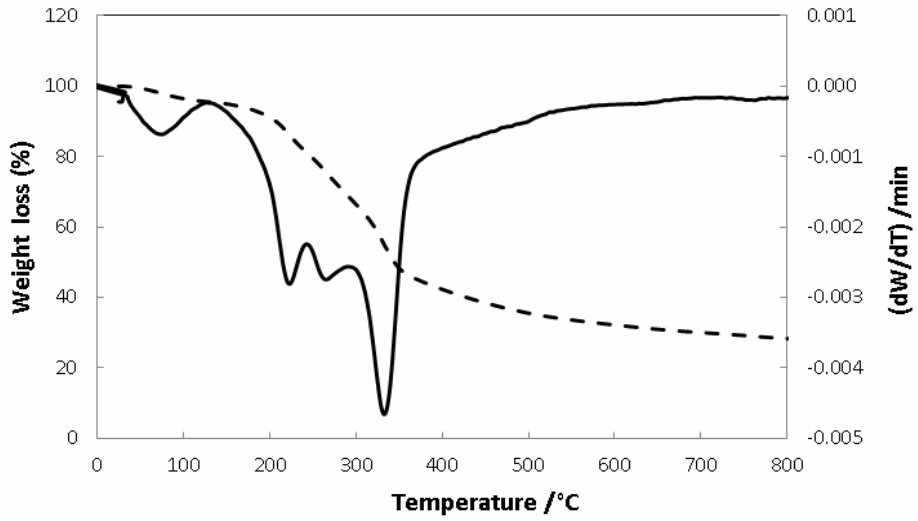

Fig. 1. (- - - -) TG and (—) DTG curves of raw material used in the present study.

studies on C, H, N, O elemental analysis, reported in the literature [10-13].

Thermo-gravimetric analysis of the raw material in Fig. 1 revealed that major thermal decomposition occurred around 250-400 °C. Initial weight loss in thermo-gravimetric (TGA) curves (58.33 °C) corresponds to moisture removal, followed by a second degradation event around 330 °C, where the evolution of light volatile compounds occurs from the degradation of cellulose and hemicelluloses. On the other hand, the activation temperature of 600 °C was suggested for raw materials from the TG study, since the curve shows a straight line, which means a stable state.

XRD patterns of the raw material and activated carbon

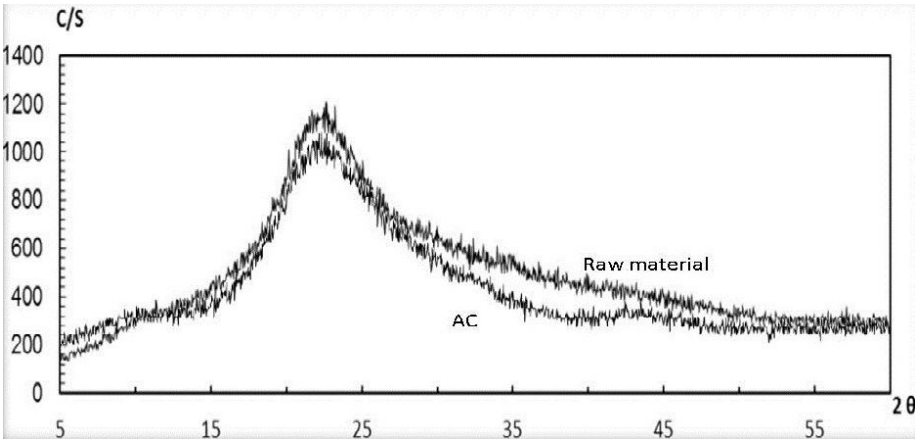

Fig. 2. XRD spectra of the raw material and activated carbon.

in Fig. 2 reveal the amorphous structure of all two samples. Activated carbon relatively known as amorphous carbon shows a very disordered microcrystalline structure due to random translation and rotation of layer planes along the c-axis. Raw materials present higher intensity of diffraction peaks. The differences in the XRD patterns are caused by the lowering of crystallites of the AC, during the activation process [14].

The most widely used commercial activated carbons have a specific surface area between 600-1200 (m^2 g^{-1}). The pore volume and surface area affect the size and the amount of the adsorbed molecules, respectively [15]. Porous structure of the prepared activated carbon in Table 1 shows that AC has a high surface area (1253 m^2 g^{-1}), which is favorable for the adsorption. Different surface area values and distribution of pores for lignocelluloses' materials have been reported in the literature. The difference between surface area values is due to the differences in the type of starting materials and activation method [16-20]. Figure S1 shows the pore size distribution of activated carbon calculated by N_2 adsorption data. The maximum incremental surface area and pore volume were observed at a pore width of 1-1.5 nm (micropore range of pore width). This result deduced the obtained activated carbon is composed of mostly micropores.

The representative microscopy images of the raw material and activated carbon are given in Fig. 3. The SEM image shows the homogeneous and relatively smooth surface of the activated carbon. Figure 3b also indicates the AC surface appears to be more damaging with many cavities, indicating the development of pore structure after the activation process. Most of the pores were enlarged to the range of 10-20 μm. These big pores were favorable for the diffusion of big molecules into the activated carbon. It is known that phosphoric acid causes chemical changes in the precursor facilitating formation of activated carbon at lower temperatures.

FT-IR spectrum analysis was used to investigate variation in the functional groups during activation. FT-IR spectra for the raw material and activated carbon are presented in Fig. S2. As can be observed, the activated carbon spectrum exhibits fewer absorption bands than the raw material spectrum, mainly between 3300-3400, 1000-1700, and 1300 cm^{-1}, indicating that some functional groups present in the raw material has been disappeared after the carbonization and activation steps. FT-IR investigation also revealed the presence of various functional groups and reactive atoms, including the carboxylic acid and hydroxide group the with proton exchange ability. The FT-IR spectrum of the activated carbon in Fig. S2 showes adsorption peaks around 3000-3500 cm^{-1}, indicative of the existence of bonded hydroxyl groups. The peak around 1300 cm^{-1} is due to C-C. The peak observed at 1640 cm^{-1} is due to C=N and the peak around 1051 cm^{-1} can be assigned to the C-O group. These results have been show various surface functional groups include aromatic C=C stretching,

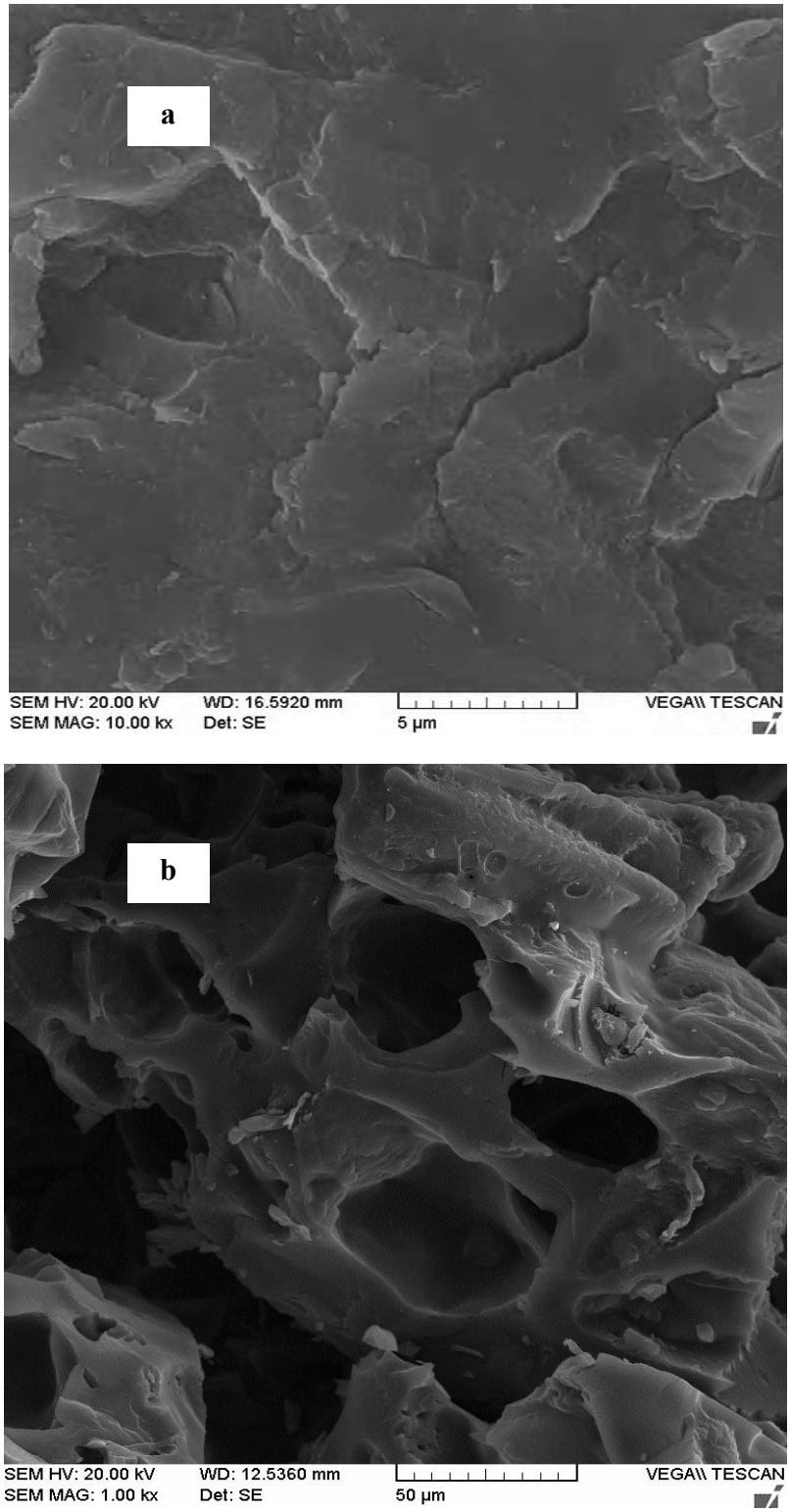

Fig. 3. SEM images of (a) raw material and (b) activated carbon.

Table 2. Porous Structure Parameters of Prepared Activated Carbon

V_t (m^3 g^{-1})	0.651
V_{micr} (m^3 g^{-1})	0.410
V_{meso} (m^3 g^{-1})	0.240
S_{BET} (m^3 g^{-1})	1243
S_{meso} (m^3 g^{-1})	420.0
S_{micr} (m^3 g^{-1})	823.0
Av pore diameter (nm)	0.530

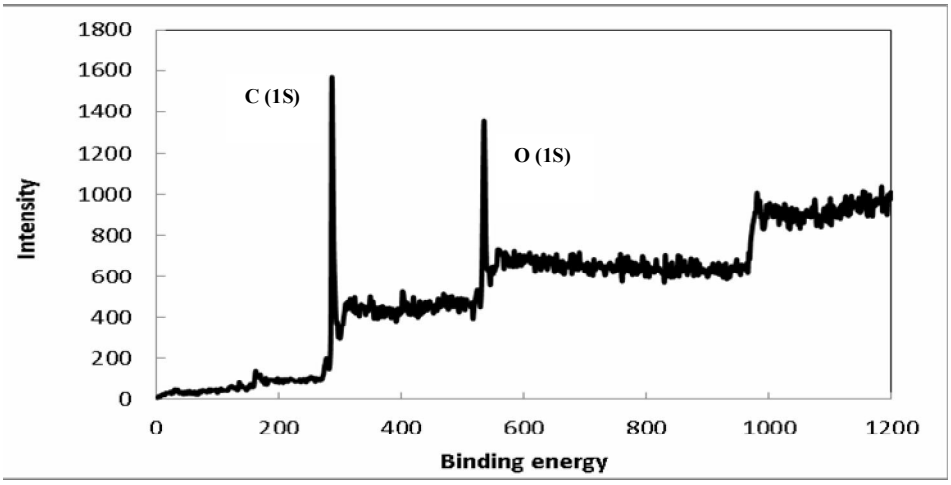

Fig. 4. C1s and O1s XPS spectra of the activated carbon.

carboxylic acid, lactone, ether bridge, quinine; phenol, and alcohol have been identified on activated carbon. These surface functional groups play a key role in the surface chemistry of activated carbon and especially in the adsorption of reagents. Also, some FT-IR assignments of functional groups on carbon surface are listed in Table 4.

In the present work total acidity and basicity of adsorbent were characterized using pH at the point of zero charge and Bohem titration. Value of pH_{zpc} 3.73 showed predominance of acidic groups on AC surface, which have been reported as being the carboxylic, lactonic, and phenolic groups. The results of Boehm titration in Table 5 showed that AC has approximately 0.8 (mmol g^{-1}) of basic group and 0.94 (mmol g^{-1}) of the acid group on its surface. The acid groups are due to lactonic (0.37 mmol g^{-1}), phenolic groups (0.74 mmol g^{-1}), and carboxylic group (0.03 mmol g^{-1}).

To assess the chemistry of the surface layers, the AC under this study were analyzed by XPS and the O(1s) and C(1s) spectra were obtained (see Fig. 4). The O(1s) and C (1s) spectra were convoluted according to the experimental procedure and quantified functional groups are summarized in Table 6.

The TPD result of studying activated carbon is given in Fig. 5. TPD analyses were carried out to quantify the oxygen functional groups present in the AC (see Table 3).

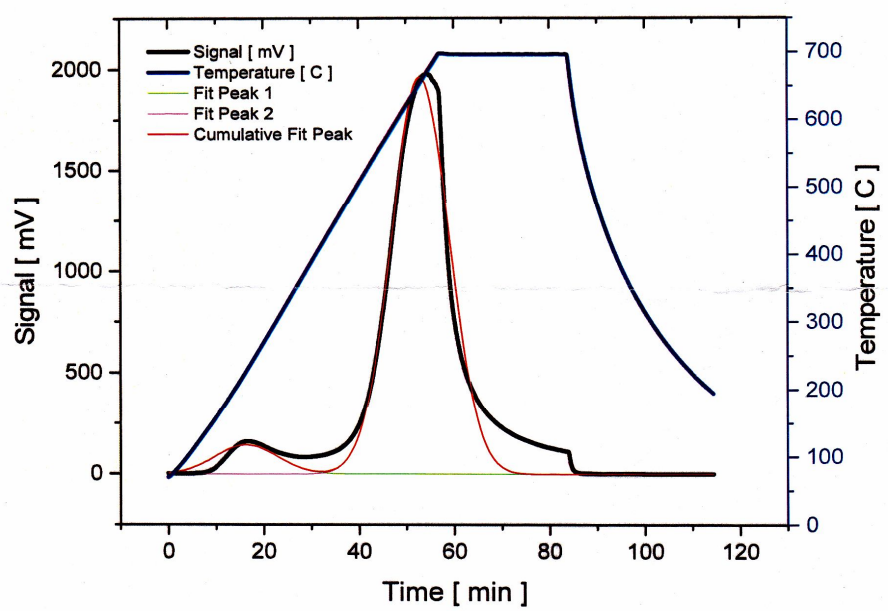

Fig. 5. TPD curve for the activated carbon.

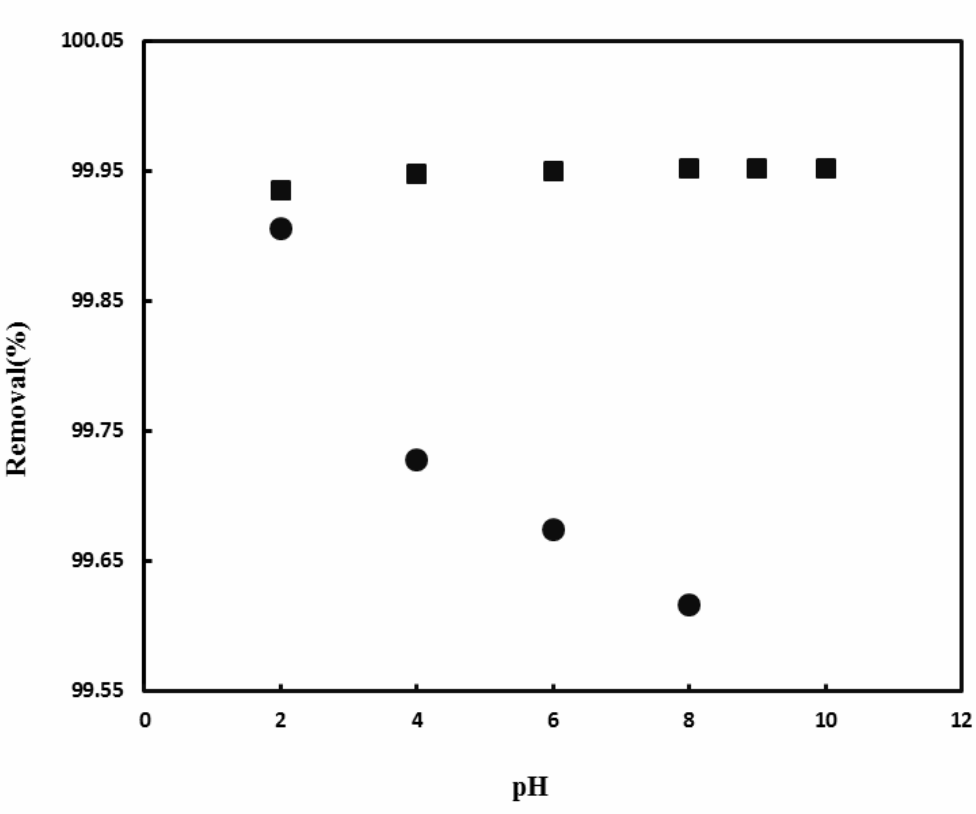

Fig. 6. Effect of solution pH on the removal of (■) methylene blue; (●) methyl orange on AC.

The CO_2 profiles shows the first maximum in the temperature 239.7 °C, which is very likely due to the decomposition of carboxylic groups and the second maximum appears in 653.051 °C, which originates from the more stable anhydrides or lactone groups [26]. Comparing the results obtained by Bohem titration, XPS ad TPD shows a good agreement for the kind of oxygen functional group found for prepared activated carbon. On the other hand, no apparent agreement was found between the quantitative results obtained by XPS, TPD and Bohem methods, due to the limitations of the Boehm titration method and the presence of porosity [27].

Adsorption of Azo Dyes onto Activated Carbon

Effect of pH, time, adsorbent dose, initial concentration and temperature. The plots in Fig. 6 confirm that adsorption of MO is strongly influenced by pH, which is explained based on the point of zero charge (PZC). In the present study, the pH values for the zero charged activated carbon were found to be approximately pH = 3.73. Therefore, at lower than pH_{pzc}, the adsorbent surface has a positive charge and adsorbs the methyl orange dyes via electrostatic attraction. On the other hand, at pH higher than pH_{pzc}, the adsorbent surface has a negative charge and adsorbs the methylen blue dye *via* electrostatic attraction. A similar behavior was observed for the adsorption of methylene violet and methyl orange onto Phragmites australis [28].

The kinetic of dyes adsorption onto activated carbon in Fig. 7 shows that the extent of adsorption is rapid during the initial stages, becoming slow during the later stages until saturation is achieved. It was found that more than 87% of MO and 97% of MB removal occurres in the first 10 min at initial concentrations. This shows that equilibrium can be assumed to be achieved after 20 min-equilibrium being basically due to the saturation of the active site and slow pore diffusion, at which time further adsorption cannot take place [29].

The effect of the adsorbent dose on the removal of the MO and MB is presented in Fig. 8. It was observed that the removal percentage increases rapidly at first with the increase in adsorbent dose till 0.05 g and after the critical dose the removal percentage almost reaches a constant value. This can be attributed to increase the adsorbent surface area and availability of more adsorption sites with increasing dosage of the adsorbent, while the adsorption density of dye decreased when the adsorbent dosage was increased [30].

The data presented in Fig. 9 showed that adsorption of MO and MB is increased with increases in temperature, which is typical for endothermic adsorption. The increase in adsorption with increasing temperatures suggests strong adsorption interactions between adsorbent surfaces and the dye molecules.

The results related to the effect of the initial MO and MB concentrations on the adsorption rate are given in Fig. 10. The amount of adsorption increased for both dyes when the initial concentration was changed. The single, smooth, and continuous curve of these compounds can be ascribed to the S_2 type, according to the Giles classification scheme [31].

In the present work, the Langmuir [32], Freundlich[33], and Temkin isotherms [34] were used to analyze the experimental equilibrium data. The linear form of these models are presented in Eqs. (3)-(5).

The Langmuir isotherm was developed by Irving Langmuir in 1916 to describe the pressure dependence to surface coverage and gas pressure at a fixed temperature. The linear form of this model is presented as follows:

$$\frac{C_e}{q_e} = \frac{1}{K_L Q_m} + \frac{C_e}{Q_m} \quad (3)$$

where K_L is the Langmuir adsorption constant (l mg^{-1}) and Q_m is the theoretical maximum adsorption capacity (mg g^{-1}). These parameters were obtained from slope and intercept of a linear plot of (C_e/q_e) *vs*. C_e. The values for the adsorption capacity, adsorption constant and the correlation coefficient show that the AC has a good adsorption capacity for MO and MB as compared to some data obtained from the literature (see Table S1). Also activated carbon with negative surface charge is better adsorbent for MB.

The correlation coefficient (R^2) of 0.99 indicates that this isotherm is suitable for adsorption prediction. Theoretical maximum adsorption capacity in Table 7 is near to the experimental adsorbed amounts and corresponds closely to the adsorption isotherm plateau, indicating that the modeling of Langmuir for the adsorption system is the

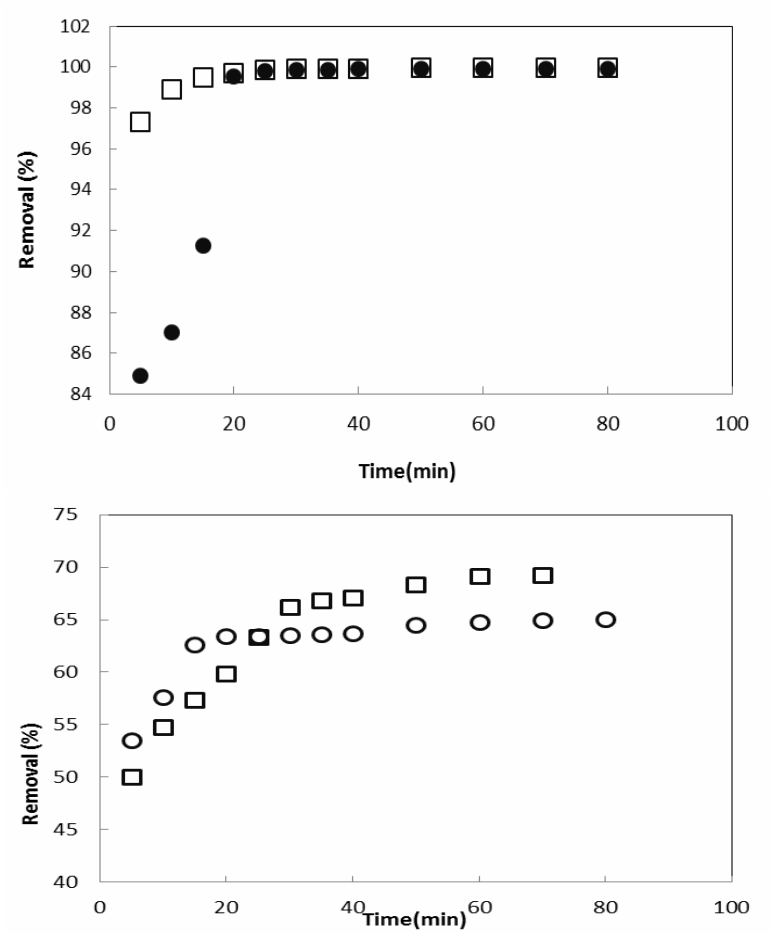

Fig. 7. Effect of contact time on the removal of (□) methylene blue; (●) methyl orange on AC.

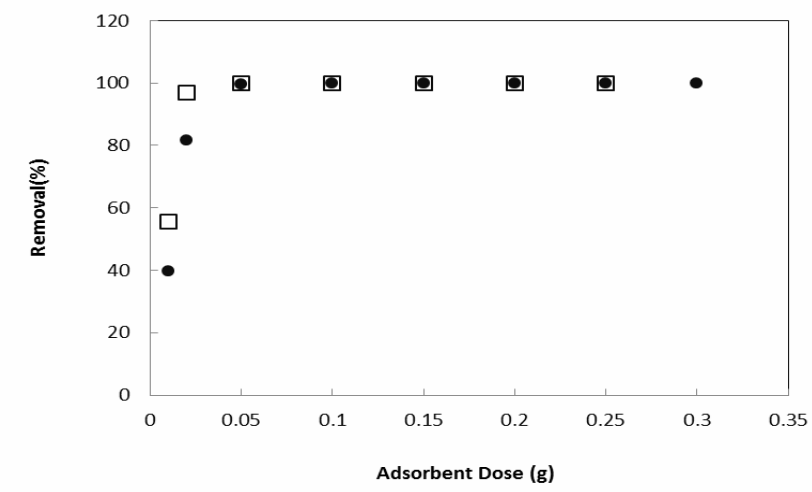

Fig. 8. Effect of adsorbent dose on the removal of (□) methylene blue; (●) methyl orange on AC.

Table 3. Results of TPD Analysis

(CO_2) (μmol g^{-1})	
Temperatures (°C)	Group decomposed
100-400	Carboxilic
200-400	Lactone
400-600	Anhydride

Table 4. Results of FT-IR Analysis

	FT-IR results		
Functional group	Present work	Reference wave number	Ref.
C= O (stretching)	1726	1720	[21]
O-H	3471	3500	[22]
Quinones	1574	1550-1680	[23]
C-OH (stretching)	1051	1000-1220	[23]
O-H (Alcohol/Phenol O-H Stretch)	3471	3500	[22]
Lactones (C-O stretching)	1726	1720	[21]
Ketones (C= O stretching)	1574	1570	[24]

Table 5. Results of Bohem Method

Bohem titration	
Basic content (mmol g^{-1})	0.82
Phenolic	0.74
Carboxilic	0.03
Lactonic	0.37

best fitting model.

The Freundlich isotherm based on the well-known assumption for adsorption on heterogeneous surfaces can be expressed in the linear form as follows:

$$\log q_e = \log K_f + \frac{1}{n}\log C_e \quad (4)$$

where n is the Freundlich constant related to adsorption intensity (which indicates how favorable the process is) and

Table 6. Results of XPS Analysis

XPS analysis (%)			
ev	Functional group	ev	Functional group
C(1s)		O(1s)	
284.4	C=C	531.1	C=O
285.2	C (aliphatic)	532.2	C-OH;C-O-C
286	C-OH;C-O-C	533.3	COOCO
287.1	C=O	534.2	COOH
288.5	COOH;COOC	535.9	Adsorbed H_2O

Table 7. Isotherm Constant and Correlation Coefficients Calculated for MO and MB Adsorption

Isotherm	Parameters	Methyl orange	Methylen blue
	Q_m (mg g^{-1})	66.32	384.0
Langmuir	K_a (l mg^{-1})	1.000	50.00
	R^2	1.000	1.000
	1/n	0.920	2.830
Freundlich	K_f (l mg^{-1})	62.17	2.830
	R^2	0.910	0.990
	B_1	12.43	32.70
Tempkin	K_T (l mg^{-1})	286.4	3075
	R^2	1.000	0.970
	Q_m (exp.)	62.00	398.0

K_f is the Freundlich constant related to the relative adsorption capacity of the adsorbent when the adsorption process is favorable, 1/n is between 1-10. Also, the ratio 1/n provides information related to the surface heterogeneity. The values of K_f and 1/n were extrapolated from the intercept and slope of plot of $\ln q_e$ *vs*. $\ln C_e$. In the current study, the 1/n value for activated carbon, indicating that activated carbon has a high degree of heterogeneity and is a suitable adsorbent for azo dyes.

In a similar manner, the Temkin and Pyzhev isotherm, in terms of a dimensionless binding energy (K_T), may be presented as follows

$$q_e = B_1 \ln K_T + B_1 \ln C_e \quad (5)$$

This isotherm takes into account the indirect adsorbate-adsorbate interactions on adsorption isotherms. In Eq. (5), K_T is the binding energy of adsorbent and adsorbate,

Table 8. Kinetic Constant and Correlation Coefficients Calculated for MO and MB Adsorption

	Parameter	MO	MB
	q_e (cal.)	8.92	1.30
First-order	$K_1 \times 10^{-3}$ (l min^{-1})	0.06	6.39
	R^2	0.94	0.99
	q_e (cal.)	76.0	400
Second-order	$K_2 \times 10^{-3}$ (l min^{-1})	0.01	0.30
	R^2	1.00	1.00
	b	0.10	1.79
Elovich	*a*	785.	276
	R^2	0.89	0.95
	K_{dif} (l min^{-1})	4.69	0.27
	C	51.8	33.6
Intraparticle	R^2	0.86	0.85
	$q_{e\ (exp.)}$	74.9	398.9
	$q_{m\ (exp.)}$	62.0	398
		Raw material	
	q_e (cal.)	1.320	4.170
First-order	$K_1 \times 10^{-3}$ (l min^{-1})	0.008	0.040
	R^2	0.930	0.960
	q_e (cal.)	65.35	71.40
Second-order	$K_2 \times 10^{-3}$ (l min^{-1})	0.016	0.004
	R^2	0.999	0.996
	b	0.230	0.125
Elovich	*a*	675.0	720.0
	R^2	0.830	0.960
Intraparticle	K_{dif} (l min^{-1})	2.020	3.490
	C	53.33	44.60
	R^2	0.650	0.920
	$q_{e\ (exp.)}$	65.01	73.14

Table 9. Thermodynamic Parameters for MO and MB Adsorption onto Activated Carbon

Temperature		293.15	303.15	313.15	323.15	333.15	338.15
Methylene blue	K°	9.17871	34.9000	121.3512	176.504	226.774	334.150
	ΔG° (kJ mol^{-1})	-368.624	-738.384	-1196.889	-1505.3	-1803.79	-2174.29
Methyl orange	K°	361.962	377.768	383.3477	384.76	386.199	386.199
	ΔG° (kJ mol^{-1})	-14351.8	-14702.6	-14986.23	-15243	-15500.1	-15747.7

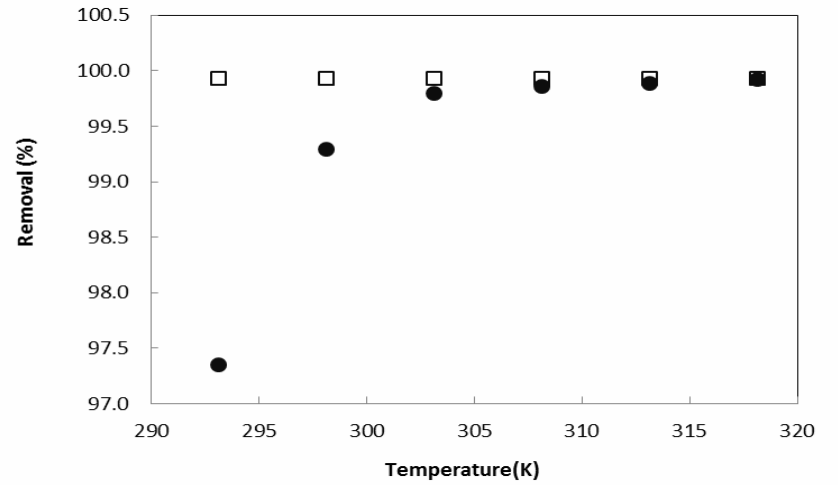

Fig. 9. Effect of temperature on the removal of (□) methylene blue; (●) methyl orange on AC.

B_1 (= *RT/b)* is related to the heat of adsorption, T is the absolute temperature in Kelvin, and R is the universal gas constant (8.314 J K^{-1} mol^{-1}). In endothermic and exothermic adsorption reactions, the value of B_1 is higher and lower than unity, respectively. Values of B_1 and K_T were calculated from the plot of q_e against lnC_e (see Table 7).

The reported value of B_1 in Table 7 indicates that the adsorption reaction of dyes onto activated carbon occurs endothermically in the concentration range studied. This fact suggests that there is an electrostatic interaction and the heterogeneity of pores on activated carbon surface plays a significant role in the adsorption of dyes. By comparing the experimental results with equilibrium isotherm equations, it was found that Langmuir, Freundlich, and Temkin isotherms are all well fitted with the experimental data. However, the Langmuir isotherm achieved the best fit.

Adsorption kinetics

Adsorption kinetics governs the solute uptake rate, measures the adsorption efficiency of the adsorbent, and determines its applicability for explaining the experimental data. Firstly, the adsorption rate of the sorbents was analyzed using Lagergren's first-order rate equation in linear form as follows [43]:

$$\log(q_e - q_t) = \log(q_e) - \frac{k_1}{2.303t} \quad (6)$$

where q_e and q_t are adsorption capacity at equilibrium and at time t, respectively; and k_1 is the rate constant of pseudo first-order adsorption (min^{-1}). Values of k_1 and q_e can be determined from the slope and intercept of the plot of log (q_e - q_t) *vs.* t, respectively. The data in Table 8 show that the

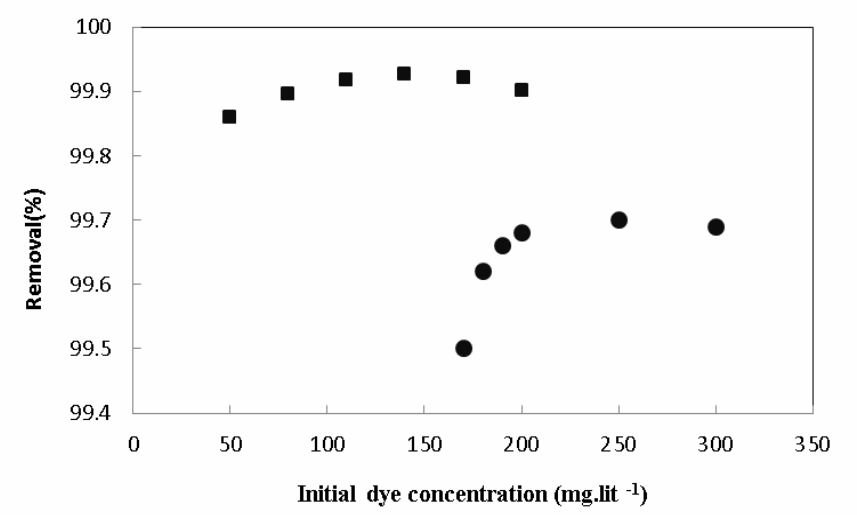

Fig. 10. Effect of initial concentration on the removal of (■) methylene blue; (●) methyl orange on AC.

pseudo first-order adsorption rates are not suitable to describe the experimental data, considering the range of values for R^2 and the fact that the greatest gap appeared between the experimental and theoretical q_e values.

The pseudo second-order model [43] with well-known Eq. (7) was tested to analyze and evaluate the efficiency of experimental

$$\frac{t}{q_t} = \frac{1}{k_2 q_e^2} + \frac{1}{q_e(t)} \quad (7)$$

Where k_2 is the equilibrium rate constant of pseudo second-order adsorption (g mg^{-1} min^{-1}).

Adsorption processes include adsorbate movement from bulk solution to the adsorbent (bulk diffusion), migration of adsorbate through the film to the entrances of the pores (film diffusion), pore diffusion or intraparticle diffusion and adsorption at the available adsorption site on the surface of pores. In the pseudo second-order model, the rate-limiting step is the surface adsorption that involves chemisorption, where the removal from the solution is due to physicochemical interactions between two phases. The advantages of pseudo-second-order equation are: calculation of adsorption capacity, initial adsorption rate and the rate constant without knowing any parameter.

The experimental kinetic data were adjusted according to the indicated model. The results of R^2, k_2 and q_e in Table 8 showed that the pseudo second-order model provides the best correlation with experimental results. The calculated adsorption capacity is also near the experimental adsorbed amount indicating that the pseudo second-order model for the adsorption system is acceptable. According to the pseudo-second order, this suggests that this sorption system based on the assumption that the rate-limiting step may be chemical sorption or chemisorptions involving valence forces through sharing or exchanging electrons between dyes ions and activating sites of AC.

The Elovich equation was developed to describe adsorption capacity and is generally expressed as linear form:

$$q_t = \frac{1}{\beta}\ln(\alpha\beta) + \frac{1}{\beta}\ln(t) \quad (8)$$

where q_t is the amount of adsorbed lead by adsorbent at a time t, α is the initial dye adsorption rate (mg g^{-1} min^{-1}) and β is desorption constant (g mg^{-1}) during any one experiment. The general explanations for this form of kinetic equation involve variations of chemisorption energy, in which the active sites are heterogeneous in the adsorbent. This supports that the heterogeneous sorption mechanism is likely responsible for the uptake of the dyes. The Elovich

model basically supports chemisorption; the Elovich plots of q_t *vs.* ln(t) yield a linear relationship. The reported parameters in Table 8 show the lack of success for the Elovich model.

The last applied alternative kinetic model in this study is intraparticle diffusion model [43]. The intraparticle diffusion model describes adsorption processes based on the sorbate diffuses towards adsorbent (*i.e.*, the process is diffusion controlled), as depicted by Eq. (9):

$$q_t\ K_{dif^{t\ 1/2}} + C \tag{9}$$

The calculated values of K_{dif} and C from the slope and intercept of q_t *vs.* $t^{1/2}$ are reported in Table 3. Intraparticle diffusion is the sole rate-limiting step, when the plot of q_t *vs.* $t^{1/2}$ passes through the origin and the value of C (in this case) is equal to zero. This phenomenon shows that the intraparticle diffusion model may be a controlling factor in determining the adsorption kinetics. The distance of R^2 values (Table 8) from unity for adsorption of lead on AC indicates the non-applicability of this model that rejects the rate-limiting step in the intraparticle diffusion process. As already mentioned, the adsorption mechanism for any dye removal by an adsorption process may be assumed to involve the following four steps: (i) bulk diffusion; (ii) film diffusion; (iii) pore diffusion or intraparticle diffusion; (iv) adsorption of dye on the sorbent surface. Previous studies showed that such plots may present a multi-linearity [43], which indicates that two or moresteps occur. The first, sharper portion is the external surface adsorption or instantaneous adsorption stage. The second portion is the gradual adsorption stage, where the intraparticle diffusion is rate-controlled. The third portion is the final equilibrium stage where the intraparticle diffusion starts to slow down due to extremely low solute concentrations in the solution.

In general, the kinetics of azo dyes adsorption onto the activated carbon were best described by the pseudo second-order model based on the correlation coefficient values for all three equations. Adsorption thermodynamics.

The adsorption thermodynamic parameter, *i.e.*, Gibbs free energy change for adsorption, was calculated using the following equation [43]:

$$\Delta G^\circ = -RT\ln K_c \tag{10}$$

where R is the universal gas constant (8.314 J mol^{-1} K^{-1}), T is the temperature (K), and K_C is the equilibrium constant. Values of K_C may be calculated from the relation $\ln q_e/C_e$ *vs.* q_e at different temperatures and extrapolated to zero. The calculated thermodynamic parameters are listed in Table 9. The negative ΔG° values confirm the spontaneous nature and feasibility of the adsorption process. The standard entropy and enthalpy change for adsorption can be calculated from the slope and intercept of lnK° *vs.* 1/T by using the Van't Hoff equation.

$$\ln K^\circ = \left(\frac{\Delta S^\circ}{R}\right) - \left(\frac{\Delta H^\circ}{RT}\right) \tag{11}$$

The positive value of ΔH° reflects endothermic adsorption of dyes onto the adsorbents, while the positive value of (ΔSº) indicates an increase in the degree of freedom (or disorder) of the adsorbed
species.

CONCLUSIONS

The removal of methyl orange and methylene blue from aqueous solution was studied using activated carbon. Persian Mesquite Grain can be effectively used as a raw material for the preparation of adsorbent. The integration of the results obtained by FT-IR, Boehm method, XPS and TPD enabled the provision of unique information about the surface chemistry of the sample. This paper also demonstrates prepared novel adsorbent in terms of very low equilibrium time and high adsorption capacity for methyl orange and methylene blue. The kinetics of the adsorption processes can be successfully fitted to the pseudo second-order model. The calculated thermodynamic adsorption parameters showed that adsorption of both dyes onto the activated carbon was spontaneous and endothermic under the experimental conditions.

ACKNOWLEDGEMENTS

The authors are grateful for the financial support (Grant number: 32/1012) from the Research Councils of Ilam University.

REFERENCES

[1] Vukcevic, M. M.; Kalijadis, A. M.; Vasiljevic, T. M.; Abic, B. M.; Lausevic, Z. V.; Lausevic M. D., Production of activated carbon derived from waste hemp (Cannabis sativa) fibers and its performance in pesticide adsorption. *Micropor. Mesopor. Mater.* **2015**, *214*, 156-165, DOI: 10.1016/j.micromeso. 2015.05.012.

[2] Aysu, T.; Kucuk, M. M., Removal of crystal violet and methylene blue from aqueous solutions by activated carbon prepared from Ferula orientalis. *Int. J. Environ. Sci. Technol.* **2015**, *12*, 273-284, DOI: 10.1007/s13762-014-0623-y.

[3] Wang, Z., Efficient adsorption of dibutyl phthalate from aqueous solution by activated carbon developed from phoenix leaves. *Int. J. Environ. Sci. Technol.* **2015**, *12*, 1923-1932, DOI: 10.1007/s13762-014-0554-7.

[4] El-Hendawy, A. A.; Alexander A. J.; Andrews, R. J.; Forrest, G., Effects of activation schemes on porous, surface and thermal properties of activated carbons prepared from cotton stalks. *J. Anal. Appl. Pyrol.* **2008**, *82*, 272-278, DOI:10.1016/j.jaap.2008.04.006.

[5] Manoj Kumar Reddy, P.; Krushnamurty, K.; Mahammadunnisa, S. K.; Dayamani, A.; Subrahmanyam, C. H., Preparation of activated carbons from bio-waste: effect of surface functional groups on methylene blue adsorption. *Int. J. Environ. Sci. Technol.* **2015**, *12*, 1363-1372, DOI: 10.1007/ s13762-014-0506-2.

[6] Kant, R., Textile dyeing industry an environmental hazard. *Nat. Sci.* **2012**, *4*, 22-26. DOI: 10.4236/ ns.2012.41004

[7] Rengarag, S.; Arabindoo, B.; Murugesan, V., Activated carbon from rubber seed and palm seed coat, preparation and characterization. *J. Sci. Ind. Res.* **1999**, *6*, 57, 129-132.

[8] Rengarag, S.; Seung-Hyeon, M.; Sivabalan, S.; Arabindoo, B.; Murugesan, V., Agricultural solid waste for the removal of organics: Adsorption of phenol from water and wastewater by palm seed coat activated carbon. *Waste Manage.* **2002**, *22*, 543-548, DOI: 10.1016/S0956-053X(01)00016-2.

[9] Yang, T., Characteristics of activated carbons prepared from pistachio-nut shells by potassium hydroxide activation. *Micropor. Mesopor. Mater.* **2003**, *63*, 113-124, DOI: 10.1016/S1387-1811(03)00456-6.

[10] Rao, M. M.; Rao, G. P. C.; Seshaiah, K.; Choudary, N. V.; Wang, M. C., Activated carbon from Ceiba pentandra hulls, an agricultural waste, as an adsorbent in the removal of lead and zinc from aqueous solutions. *Waste Manage.* **2007**, *28*, 849-858. DOI: 10.1016/j.wasman.2007.01.017.

[11] Tsamba, A. J.; Yang, W.; Blasiak, W., Pyrolysis characteristics and global kinetic of coconut and cashew nut shells. *Fuel Process. Technol.* **2006**, *87*, 523-530. DOI: 10.1016/j.fuproc.2005.12.002.

[12] Srikanth, S.; Das, K.; Ravikumar, B.; Rao, D. S.; Nandakumar, K.; Vijayan, P., Nature of fire deposits in a bagasse and groundnut shell fire 20 mw thermal boiler. *Biomass Bioenergy,* **2004**, *75*, 273-384. DOI: 10.1016/j.biombioe.2004.03.004.

[13] Timura, S.; Cem Kantarlib, I.; Onenca, S.; Yanika, J.; Characterization and application of activated carbon produced from oak cups pulp. *J. Anal. Appl. Pyrol.* **2010**, *89*, 129-136, DOI: 10.1016/j.jaap.2010.07.002.

[14] Gomez-Serrano, V.; Cuerda-Correa, E. M.; Fernández-Gonzalez, M. C., Preparation of activated carbons from chestnut wood by phosphoric acid-chemical activation: Study of microporosity and fractal dimension. *Materials Lett.* 2005, *59*, 846-853, DOI: http://dx.doi.org/10.1088/0964-1726/14/2/010.

[15] Lartley, R. B.; Acquah, F., Developing national capability for manufacture of activated carbon from agricultural waste. *Ghana Engineer.* 1999, *5*.

[16] Munoz, Y.; Arriagada, R.; Soto-Garrido, G.; Garcia, R., Phosphoric and boric acid activation of pine sawdust. *J. Chem. Technol. Biotechnol.* **2003**, *78*, 1252-1258. DOI: 10.1002/jctb.923.

[17] Patnukao, P.; Pavasant, P., Activated carbon from Eucalyptus camaldulensis Dehn bark using phosphoric acid activation. *Bioresource Technol.* **2008**, *99*, 8540-8543, DOI: 10.1016/j.biortech.2006.

10.049.

[18] Guo, Y.; Rockstraw, D. A.; Physicochemical properties of carbons prepared from pecan shell by phosphoric acid activation. *Bioresource Technol.* **2007**, *98*, 1513-1521, DOI: 10.1016/ j.biortech.2006.06.027.

[19] Yang, T.; Lua, A. C., Characteristics of activated carbons prepared from pistachio-nut shells by potassium hydroxide activation. *Micropor. Mesopor. Mater.* **2003**, *63*, 113-124, DOI: 10.1016/S1387-1811(03)00456-6.

[20] Moreno-Castilla, C.; Carrasco-Marin, F.; Lopez-Ramon, M. V.; Alverez-Merino, M. A.; Chemical and physical activation of olive-mill waste water to produce activated carbons. *Carbon,* **2001**, *39*, 1415-1420, DOI: 10.1016/S0008-6223(00)00268-2.

[21] Kazmierczak, J.; Biniak, S.; Swiatkowski, A.; Radeke, H., Interdependence of different parameters characterizing the chemistry of an activated carbon surface. *J. Chem. Soc. Farad. T1.* **1991**, *87*, 3557-3561, DOI: 10.1039/FT9918703557.

[22] Vasu, A. E., Surface modification of activated carbon for enhancement of nickel(II) adsorption. *Eur. J. Chem.* **2008**, *5*, 814-819, DOI: http://dx.doi.org/10.1155/2008/610503.

[23] Fanning, P. E.; Vannice, M. A., A DRIFTS study of the formation of surface groups on carbon by oxidation. *Carbon,* **1993**, *31*, 721-730, DOI: 10.1016/0008-6223(93)90009-Y.

[24] Biniak, S.; Szymanski, G.; Siedlewski, J.; Swiatkowski, A., The characterization of activated carbons with oxygen and nitrogen surface groups. *Carbon,* **1997**, *35*, 1799-1810, DOI: 10.1016/S0008-6223(97)00096-1.

[25] Lambert, J. B.; Shurvell, H. F.; Verbit, L.; Cooks, R. G.; Stout, G. H., Organic Structural Analysis, Macmillan. New York, 1976.

[26] Saleh Shafeeyan, M.; Mohd Ashri Wan Daud, W.; Houshmand, A.; Shamiri, A., A review on surface modification of activated carbon for carbon dioxide adsorption. *J. Anal. Appl. Pyrol.* **2010**, *89*, 143-151, DOI: 10.1016/j.jaap.2010.07.006.

[27] Kalijadis, A. M.; Vukcevic, M. M.; Jovanovic, Z. M.; Lausevic, Z. V.; Lausevic, M. D.; Characterisation of surface oxygen groups on different carbon materials by the Boehm method and temperature-programmed desorption. *J. Serb. Chem. Soc.* **2011**, *76*, 757-768, DOI: http://dx.doi.org/10.2298/JSC091224056K.

[28] Chen, S.; Zhang, J.; Zhang, C.; Yue, Q.; Li, Y.; Li, C., Equilibrium and kinetics studies of methyl orange and methyl violet adsorption on activated carbon derived from phragmites australis. *Desalination,* **2010**, *252*, 149-156, DOI: 10.1016/j.desal.2009.10.010.

[29] Rengaraj, S.; Kim, Y.; Joo, C. K.; Yi, J., Removal of copper from aqueous solution by aminated and protonated meso porous alumina. Kinetics and equilibrium. *J. Colloid Interf. Sci.* **2004**, *273*, 14-21, DOI: 10.1016/S0956-053X(01)00016-2.

[30] Kannan, N.; Sundaram, M. M., Kinetics and mechanism of removal of methylene blue by adsorption on various carbons-a comparative study, *Dyes Pigments,* **2001**, *51*, 25-40, DOI: 10.1016/S0143-7208(01)00056-0.

[31] Giles, C. H.; Smith, D. A., A general treatment and classification of the solute adsorption isotherm I. theoretical. *J. Colloid Interf. Sci,* **1973**, *47*, 755-765, DOI: 10.1016/0021-9797(74)90252-5.

[32] Langmuir, I., The constitution and fundamental properties of solids and liquids. part i. solids. *J. Am. Chem. Soc.* **1916**, *38*, 2221-2295, DOI: 10.1021/ja02268a002.

[33] Freundlich, H. M. F., over the adsorption in solution. *J. Phy. Chem.* **1906**, *57*, 385-470, DOI: 10.1016/j.biortech.2008.06.069.

[34] Temkin, M. J.; Pyzhev, V., Recent Modifications to Langmuir Isotherms, *Acta Physiochim.* RSS, **1940**, *12*, 217-222.

[35] Ghaedi, M.; Golestani Nasab, A.; Khodadoust, S.; Rajabi, M.; Azizian, S., Application of activated carbon as adsorbents for efficient removal of methylene blue: Kinetics and equilibrium study. *J. Ind. Eng. Chem.* **2014**, *20*, 2317-2324, DOI: 10.1016/j.jiec.2013.10.007.

[36] Mondal, S.; Sinha, K.; Aikat, K.; Halder, G.,

Adsorption thermodynamics and kinetics of ranitidine hydrochloride onto superheated steam activated carbon derived from mung bean husk. *J. Environ. Chem. Engin.* **2015**, *3*, 187-195, DOI: 10.1016/j.jece.2014.11.021.

[37] Hameed, B. H.; Din, A. T. M.; Ahmad, A. L., Adsorption of methylene blue onto bamboo-based activated carbon: Kinetics and equilibrium studies. *J. Hazard. Mater.* **2007**, *141*, 9-25, DOI: 10.1016/j.jhazmat.2006.07.049.

[38] Gao J. J.; Qin, Y. B.; Zhou, T.; Cao, D. D.; Xu, P.; Hochstetter, D.; Wang, Y. F., Adsorption of methylene blue onto activated carbon produced from tea. *J. Zhejiang Univ. Sci B,* **2013**, *14*, 650-658, DOI: 10.1631/jzus.B12a0225.

[39] Li, Y.; Dua, Q.; Liua, T.; Pengb, X.; Wanga, J.; Suna, J.; Wanga, Y.; Wua, S.; Wanga, Z.; Xiaa, Y.; Xia, L., Comparative study of methylene blue dye adsorption onto activated carbon, graphene oxide, and carbon nanotubes. *Chem. Eng. Res. Des.* **2013**, *91*, 361-368, DOI: 10.1016/j.cherd.2012.07.007.

[40] Danish, M.; Hashim, R.; Mohamad Ibrahim, M. N.; Sulaiman, O., characterization of physically activated acacia mangium wood-based carbon for the removal of methyl orange Dye. *Bio Resources,* **2013**, *8*, 4323-4339, DOI: 10.15376/biores.8.3.4323-4339.

[41] Mahmoudi, K.; Hamdi, N.; Srasra, E., Preparation and characterization of activated carbon from date pits by chemical activation with zinc chloride for methyl orange adsorption. *J. Mater. Environ. Sci.* **2014**, *5*, 1758-1769, DOI: 10.1021/ie050162.

[42] Pal, J.; Kanti Deb, M.; Kumar Deshmukh, D.; Verma, D., Removal of methyl orange by activated carbon modified by silver nanoparticles. *Appl. Water Sci.* **2013**, *3*, 367-374, DOI: 10.1007/s13201-013-0087-0.

[43] Ghaedi, M.; Ghayedi, M.; Nasiri Kokhdan, S.; Sahraei, R.; Daneshfar, A., Palladium, silver, and zinc oxide nanoparticles loaded on activated carbon as adsorbent for removal of bromophenol red from aqueous solution. *J. Ind. Engin. Chem.* **2013**, *19*, 1209-1217, DOI: 10.1016/j.jiec.2012.12.020.